RSC Advances

ROYAL SOCIETY OF CHEMISTRY

www.rsc.org/advances

Graphical Abstract

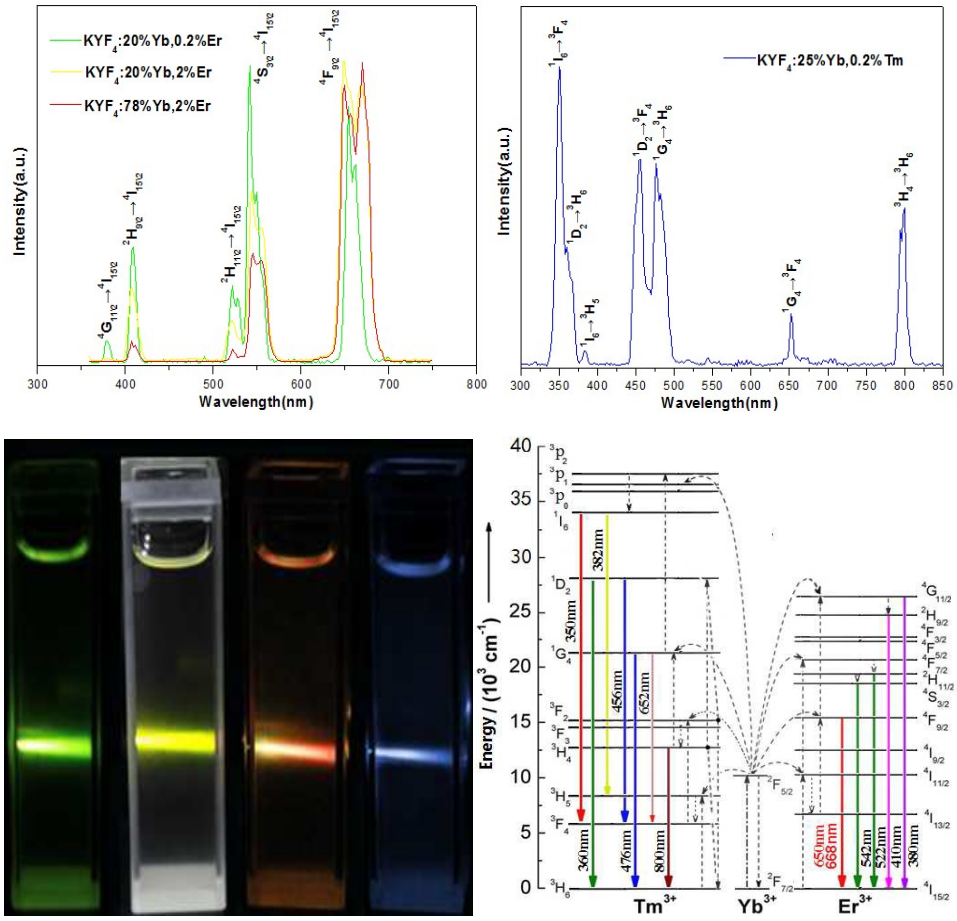

Colloidal β-KYF_4:Yb^{3+},Er^{3+}/Tm^{3+} Nanocrystals: Tunable Multicolor Up-conversion Luminescence from UV to NIR Regions

Bin ZHOU[1], Youfa Wang[2,*], Donglin XIA[3,*]

[1] School of Materials Science and Engineering, Wuhan University of Technology, Wuhan 430070, P. R. China

[2]State Key Laboratory of Advanced Technology for Materials Synthesis and Processing, Wuhan University of Technology, Wuhan 430070, P. R. China

[3] State Key Laboratory of Silicate Materials for Architectures, Wuhan University of Technology, Wuhan 430070, P. R. China

Abstract: Pure β-KYF_4 nanocrystals codoped with Er^{3+}/Yb^{3+} and Tm^{3+}/Yb^{3+} were successfully synthesized via the thermal decomposition of trifluoroacetate precursors using oleic acid and octadecylene as coordinate solvents. The up-conversion optical properties of the β-KYF_4 nanocrystals with different lanthanide (Ln)-doped ions (Yb^{3+}/Er^{3+}, Yb^{3+}/Tm^{3+}) were investigated. It is found that the colloidal dispersion of β-KYF_4:Yb,Er/Tm nanocrystals display strong multiple up-conversion emission spanning from the deep UV-to-NIR region under 980 nm excitation. Pure β-KYF_4 nanocrystals codoped with Er^{3+}/Yb^{3+} and Tm^{3+}/Yb^{3+} can emit the bright eye-visible blue, green, yellow, and red emissions by adjusting concentration of Yb^{3+} sensitizer ion and Er^{3+} or Tm^{3+}activator ions. Moreover, the UC luminescent colors can be tuned for the four colors from blue to green to yellow and finally to red emission in the

Corresponding Authors

*Youfa Wang. E-mail: wangyoufa@whut.edu.cn. Tel: 86-27-87651852.Fax:86-27-87880734

*Donglin XIA. E-mail: donglinxia@126.com. Tel/Fax: 86-27-87669729.

β-KYF_4:X%Yb^{3+}/(0.2%-2%)Er^{3+} and β-KYF_4: 25% Yb^{3+}/0.2% Tm^{3+} colloidal samples. This work substantially expands our understanding of this category of KYF_4 upconversion nanocrystals.

1. **Introduction**

Lanthanide (Ln)-doped up-conversion nanocrystals (UCNCs) have attracted considerable attention because of their potential applications in many fields such as solid-state lasers, solar cells, three-dimensional displays, infrared radiation detectors, and biomedical imaging[1-4]. Compared with traditional fluorescent materials, UCNCs exhibit excellent photostability, continuous emission capability, and sharp multi-peak line emission[5-8]. In particular, lanthanide-doped UCNCs have the remarkable ability to transfer its excitation energy states of lanthanide ions (sensitizer ion) to a neighboring ion (activator ion) to emit efficient emissions by anti-stokes process[1,9-11]. Anti-stokes process of upconverted luminescence is a nonlinear process in which low energy excited-light (near-infrared (NIR) or infrared) is converted to higher energy emitted-light (ultraviolet (UV) or visible (VIS)) through multiple sequential absorption of two or more low energy photons[5,12,13]. The anti-stokes process emerges largely due to unique intra 4f transitions and substantial energies states of the lanthanide ions, which is less influenced by the ligand field (due to the shielding of the 4f orbitals by the outer 5s and 5p orbitals) leading to sharp emission transitions[14,15].

Yb^{3+}-sensitized fluoride NCs have been believed to be one of the most efficient upconverters due to low energy lattice phonons which can minimize the quenching

effect of the excited state of lanthanide ions[16-18]. Moreover, multiple emissions in the visible region have been produced by doping multiple Ln^{3+} ions (Er^{3+} /Yb^{3+} /Tm^{3+} , Er^{3+} /Yb^{3+} or Yb^{3+} /Tm^{3+})[19,20], since these materials display a very strong effect of NIR-to-VIS photon up-conversion. Green and blue up-conversion emissions are achieved by codoping Er^{3+} and Tm^{3+}, respectively, with Yb^{3+} (as a sensitizer) in sodium host fluorides. Several research groups have recently reported up-conversion from colloids of either cubic or hexagonal $NaYF_4$ NCs[21-23]. For example, Krämer et al.[24] have identified micrometer-sized hexagonal $NaYF_4$ co-doped with Er^{3+}/Yb^{3+} or Tm^{3+}/Yb^{3+} with the highest up-conversion efficiencies, as well as hexagonal $NaGdF_4$[25] or $NaLuF_4$[5] NCs. Ln^{3+}-doped KYF_4 NCs also have been reported as one of the most efficient Ln^{3+} host for infrared (IR) to VIS UC processes. Several groups also have investigated on Er^{3+} /Yb^{3+} or Tm^{3+} /Yb^{3+} co-doped KYF_4 NCs[26-29]. The cubic phase KYF_4:Yb, Er nanocrystals were reported by Schäfer et al[26]. Intense white luminescence has also been obtained in cubic α-KYF_4:Yb^{3+}-Er^{3+}-Tm^{3+} nanocrystals by J. Méndez-Ramos et al[27]. Further, UV-VIS UC emissions containing in cubic α-KYF_4-SiO_2 doped with Eu^{3+} and co-doped with Yb^{3+} and Tm^{3+} ions have been reported by Yanes et al[28]. It can be found in the literature A few works concerning synthesis and optical properties of Ln^{3+}-doped KYF_4 cubic nanocrystals . However, the quantum yield of cubic phase nanocrystals is generally lower an order of magnitude than that of hexagonal phase. There are no further literature reports on the synthesis and optical properties of β-KYF_4:Yb,Er/Tm hexagonal nanocrystals.

The optical properties of Ln^{3+}-doped bulk KYF_4 are widely studied. However, there are few reports on the monodispersed multicolor functional KYF_4 nanocrystals with finely tuned UC emissions. It is well known that the realization of multicolor UC emissions requires the generation and intensity control of the three fundamental blue, green, and red colors. Tuning the visible color output such as three fundamental blue, green, and red colors has been reported by tuning host lattice/dopant combinations and concentration[30]. For example, $NaYF_4$ and $NaLuF_4$ NCs doped with different lanthanide activators (Er^{3+}, Ho^{3+}, and Tm^{3+}) demonstrate tunable spectra spanning visible and near-infrared regions[31,32]. However, there is no established approach to fine-tuning up-conversion emission for the UV-NIR regions by single-wavelength excitation.

Considerable efforts have been directed to the development and optimization of synthetic approaches to up-conversion nanoparticles. Schäfer et al[33] reported a solvent-free room-temperature synthesis for hexagonal $NaYF_4$ nanocrystalline. However, the solvent-free approach to small particles from bulk specimens using a readily available technique has faced challenges. Yi et al.[34] have reported the synthesis of (Yb-Er)- and (Yb-Tm)-doped hexagonal-phase $NaYF_4$ nanoparticles by decomposition of multiprecursors dissolved in oleylamine at 330°C. Herein, pure β-KYF_4 nanocrystals codoped with Er^{3+}/Yb^{3+} and Tm^{3+}/Yb^{3+} were synthesized via the thermal decomposition of trifluoroacetate precursors using oleic acid and octadecylene as coordinate solvents. The as-synthesized β-KYF_4 NCs were dispersed readily into solvent to stable colloidal solution for up-conversion emission.

In this paper, we studied the tunable multicolor up-conversion (UC) emissions using potassium host instead of traditionally used sodium host. Lanthanide (Ln)-doped up-conversion optical properties of the β-KYF_4 doped with different lanthanide doping ions (Yb^{3+}/Er^{3+}, Yb^{3+}/Tm^{3+}) were investigated. Moreover, UC mechanism and multicolor emissions control of Yb^{3+}/Er^{3+} co-doped β-KYF_4 NCs were also discussed. It is found that the colloidal dispersion of β-KYF_4:Yb,Er/Tm NCs display strong multiple up-conversion emission spanning from the deep UV-to-NIR region under 980 nm excitation. In addition, β-KYF_4 NCs could emit the bright eye-visible blue, green, yellow, and red emissions by adjusting concentration of Yb^{3+} and activator ions (Er^{3+} or Tm^{3+}). This work substantially expands our understanding of this category of KYF_4 upconversion nanocrystals.

2. Experimental section

Materials. Yttrium(III) oxide (Y_2O_3, 99.99%), Ytterbium(III) oxide (Yb_2O_3, 99.99%), Erbium(III) oxide (Er_2O_3, 99.99%), and Thulium(III) oxide (Tm_2O_3, 99.99%), potassium trifluoroacetate (CF_3COOK, ≥98%), 1-octadecene (ODE, 90%), oleic acid (OA, 90%), trifluoroacetic acid (CF_3COOH, 99.0%), Hexane (C_6H_{14}, 97%), and ethanol (CH_3CH_2OH, 99.7%). All chemicals were purchases from Aladdin Inc. and used without any further purification. Lanthanide trifluoroacetates ($(CF_3COO)_3Ln$) were prepared by dissolving the respective lanthanide oxides in trifluoroacetic acid (CF_3COOH) into a 50mL three-neck flask on a heating mantle.

Synthesis of β-KYF_4:Yb^{3+},Er^{3+}/Tm^{3+} NCs. β-KYF_4:X%Yb^{3+}/2%Er^{3+}, 20% Yb^{3+}/0.2%Er^{3+}, 25%Yb^{3+}/0.2%Tm^{3+} NCs were synthesized by thermal decomposition

of trifluoroacetate using oleic acid and octadecylene as coordinate solvents[35], including Yb^{3+} by X=20 , 35, 50, and 78 ratio instead of the host element Y^{3+}， the total mole number with lanthanide ions of each sample is 1 mmol. In a typical synthesis, the $(CF_3COO)_3Ln$ (Ln=Y, Yb, Er, and Tm), CF_3COOK (2 mmol), oleic acid (6 mL) and 1-octadecene (15 mL) were added to a 50 mL three-neck flask and stirred. The flask of oxygen and water were purged by argon bubbling at 130□ for 30min. Next, the temperature of the mixture was slowly raised to 330□ at a ramping rate of 5□/min. The reaction was held at 330□ for 1h with continuous vigorous stirring. After reaction, this stock solution was cooled to ambient temperature prior to precipitation with absolute ethanol. The NCs were isolated by precipitation with addition of 10 mL of hexane and 15 mL of ethanol followed by centrifugation at 11000 rpm for 5 min. The supernatant containing byproducts was discarded. The white precipitate was collected by centrifugation and washed with hexane and ethanol two times. Different lanthanide-doped KYF_4 NCs were dried at 60□ under the condition of vacuum.

X-ray Powder Diffraction (XRD). The X-ray powder diffraction patterns were measured by using the Bruker Discover D8 high-resolution diffractometer with CuKα radiation (λ=1.5418Å). The samples were measured at a scanning rate of 15°/min in the over the range of 2θ=10-70°.

Element Composition Analysis. The energy dispersive X-ray spectroscopy (EDS) for elemental analysis was carried out with a Hitachi S-4800 field emission scanning

electron microscope (FE-SEM). The powder samples were put on a carbon fiber copper wire mesh.

Transmission Electron Microscopy (TEM) and High-Resolution Transmission Electron Microscopy (HR-TEM). The morphology and microstructure of as-synthesized sample NCs were measured using a transmission electron microscope and high-resolution transmission electron microscopey (model JEM 2100F) equipped with a field emission gun operating at 200 KV (0.23 nm point-to-point). The colloidal NCs for TEM and HRTEM images were dispersed in an ethanol solution, subsequently one drop of the colloidal suspension was placed on carbon-coated copper grid.

Up-conversion spectra Analysis. The UC emission spectra were obtained using a 980 nm CW Ti:Sapphire laser (3900S; Spectra Physics) with an excitation power density of 0-2W/cm^2 adjustable as the excited source from a continuous-wave xenon lamp with a slit width defining spectral resolution of 1 nm. As-synthesized KYF_4 samples were uniformly dispersed in ethanol (1 wt%), and the obtained colloidal NCs were placed in 1 cm path-length quartz cuvettes (Hellma, QS). The emission signal was collected by a half-meter monochromator (HR460, Jobin Yvon) equipped with a 1200 lines/mm and detected with a CCD detector (Spectrum One, Jobin Yvon) from 300 to 850nm. UC luminescence images of the colloidal NCs were acquired with a Nikon multiple camera (model D7100) without adding any filter. All the measurements were performed at room temperature.

3. Results and discussion

3.1 Crystal Phase, Morphology and Microstructure, and Element Compositions of β-KYF_4:.Yb,Er/Tm NCs.

Fig. 1 shows the typical XRD patterns of as-prepared KYF_4 NCs co-doped with 20% Yb^{3+}/2% Er^{3+} and 25% Yb^{3+}/0.2% Tm^{3+}.

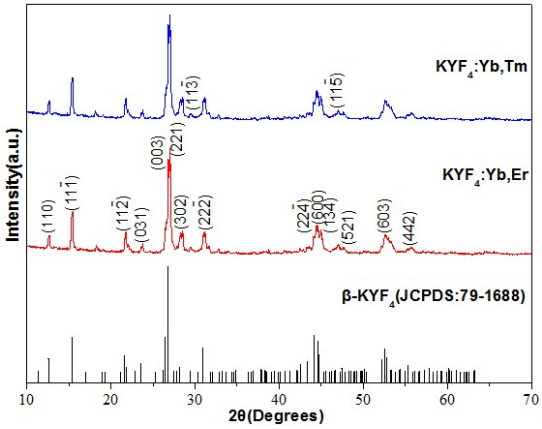

Fig.1. XRD patterns of as-synthesized KYF_4:20%Yb^{3+}, 2%Er^{3+} and KYF_4:25%Yb^{3+}, 0.2%Tm^{3+} NCs with a hexagonal crystal structure (JCPDS:79-1688).

As demonstrated in Fig.1, the XRD patterns of KYF_4:Yb,Er and KYF_4:Yb,Tm are provided with the similar diffraction peaks, which both belong to a P31(144) space group. All of the intense diffraction peaks that located at 2θ=15.5℃, 21.8℃, 27.0℃, 28.3℃, 31.2℃, 44.5℃ and 52.6℃ can easily be specified as the diffraction peaks of standard β-KYF_4 XRD patterns (JCPDS79-1688). No other miscellaneous peak is detected, which indicates the pure hexagonal KYF_4 NCs with a high crystallinity can be readily synthesized using thermal decomposition of trifluoroacetates metal-precursor method. The average nanoparticle size of KYF_4:Yb,Er and KYF_4:Yb,Tm NCs are calculated to be around 18 and 20 nm according to the Scherrer's formula $D = 0.89\lambda/(\beta\cos\theta)$, where D, λ, θ, and β are the

average particle size, X-ray wavelength (0.15405 nm), the diffraction angle and full-width at half-maximum, respectively.

The morphology and size of Yb^{3+},Er^{3+}/Tm^{3+} codoped KYF_4 NCs are analyzed by TEM and HRTEM. Fig.2 shows the TEM images of KYF_4:20% Yb^{3+}/2% Er^{3+} and KYF_4:25% Yb^{3+}/0.2% Tm^{3+} NCs, respectively. It is shown that as-synthesized KYF_4:Yb^{3+},Er^{3+}/Tm^{3+} NCs contain smaller hexagonal nanorods particles and nanoplates with good monodispersity. From Fig. 2a,b the average grain size for KYF_4:20% Yb/2% Er and KYF_4:25% Yb/0.2% Tm NCs are calculated from random 100 nanoparticle to be 16nm, 18nm, respectively , which are in good consistent to XRD analysis result calculated by scherrer's formula. The lattice fringes are obviously observed in HR-TEM images of KYF_4:Yb,Er/Tm (Fig. 2c,d), which indicated that as-synthesized KYF_4 NCs possessed highly crystallinity. The HRTEM images (Fig. 2c) of as-synthesized nanocrystals showed clear lattice fringes with a interplanar spacing of d = 0.33 nm, which corresponds to the (221) lattice plane of the hexagonal phase KYF_4. In addition, the interplanar distances of 0.21nm was also observed by HR-TEM images in Fig. 2d, corresponding to the (600) lattice planes of the hexagonal phase KYF_4, which was consistent with the XRD analysis. The corresponding elemental composition of KYF_4 codoped with 20% Yb^{3+}/2% Er^{3+} and 25% Yb^{3+}/0.2% Tm^{3+} NCs were obtained by the EDS analysis, as shown in Fig.2f. The EDS result for KYF_4:20%Yb/2%Er (Fig. 2e) demonstrates that as-synthesized NCs are mostly consist of K, Y, Yb, Er and F. The EDS result for KYF_4:25% Yb/0.2% Tm as-synthesized NCs are mostly consist of K, Y, Yb, Tm and F. Based on

the XRD and TEM analyses, it is concluded that the KYF_4 NCs with good monodispersity and small particle size can be readily controlled via the thermal decomposition of trifluoroacetate precursors.

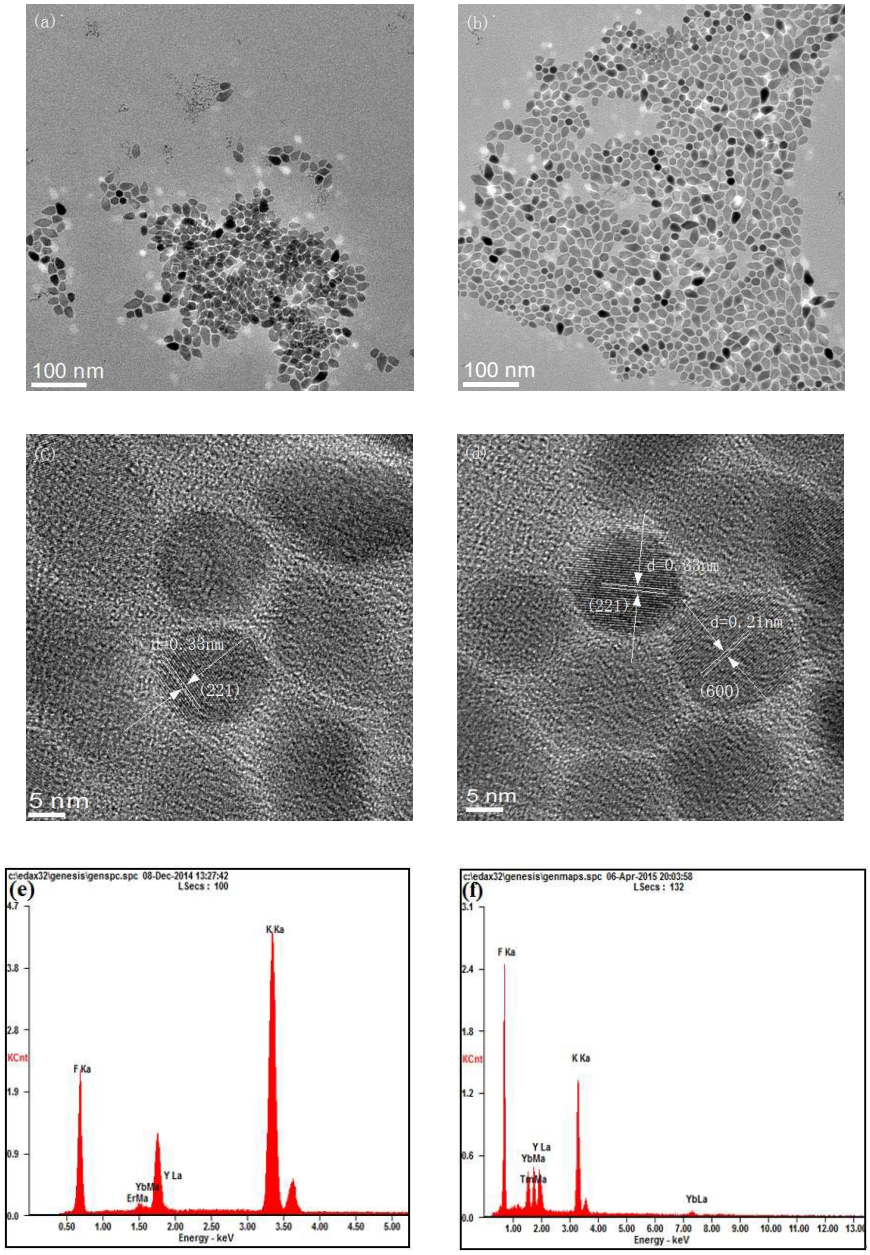

Fig.2. TEM and HRTEM images of the as-synthesized KYF_4 NCs: (a) KYF_4:20%Yb^{3+},2%Er^{3+} , (b) KYF_4:25%Yb^{3+},0.2%Tm^{3+}, (c) HRTEM image of KYF_4:20%Yb^{3+},2%Er^{3+} NCs, (d) HRTEM image of KYF_4:25%Yb^{3+},0.2%Tm^{3+} NCs, (e) EDS of KYF_4:20%Yb^{3+},2%Er^{3+} NCs, (f) EDS of KYF_4:25%Yb^{3+},0.2%Tm^{3+} NCs.

3.2 Tunability of Multicolor Up-Conversion Emissions of the β-KYF_4:.Yb,Er/Tm NCs.

Under a 980 nm laser excitation, Yb^{3+} ions are excited from the $^2F_{7/2}$ level to the $^2F_{5/2}$ level, and then transfer their energies to the nearby Er^{3+} or Tm^{3+} ions. On the basis of energy-matching conditions, the possible UC mechanisms for the β-KYF_4:Yb,Er/Tm are illustrated in Fig.3.

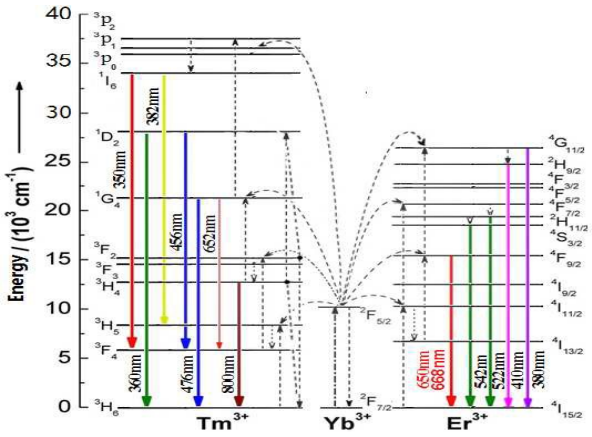

Fig.3 The simplified UC emission mechanisms of β-KYF_4:.Yb,Er/Tm

Fig.4 shows UC luminescence spectra of the different concentration Yb,Er/Tm-codoped KYF_4 NCs. As can be observed in Fig.4A, six dominant emission peaks of KYF_4 doped with different Yb and Er ion concentration centered around 668, 650, 542, 522, 410, and 380 nm, respectively. These emission peaks occurred as a result of Yb^{3+} sensitization, leading to the photon energy transfer to the nearby Er^{3+} ions. According to the simplified energy level diagram shown in Fig.3, these obvious emission peaks corresponding to 668/650, 542 and 522nm are attributed to the electronic transition of $^4F_{9/2}\rightarrow{}^4I_{15/2}$, $^4S_{3/2}$, $^2H_{11/2}\rightarrow{}^4I_{15/2}$ of the Er^{3+} ions, respectively, while emission peaks center at 410 and 380 nm correspond to electronic transitions of $^4G_{11/2}$, $^2H_{9/2}\rightarrow{}^4I_{15/2}$ of the Er ions, respectively. The relative emission peaks intensity

of the three KYF_4:Yb,Er samples affected the final luminescence performance. The intense green (542 nm) and weak red emissions (650 nm) were observed in the KYF_4:20% Yb,0.2% Er, which corresponding to the bright eye-visible green luminescence in Fig.4C. The weak green and intense red emissions centered at 542nm and 650nm were observed in the KYF_4:20% Yb, 2% Er, which corresponding to the bright eye-visible yellow luminescence solution, its transparency was shown in Fig.4D. Compared with emission for KYF_4:20%Yb,2% Er, the intense red emissions for KYF_4:78% Yb/2% Er changed from 650 nm to 680 nm with a little red shift, which corresponding to the bright eye-visible red luminescence, as shown in Fig.4E.

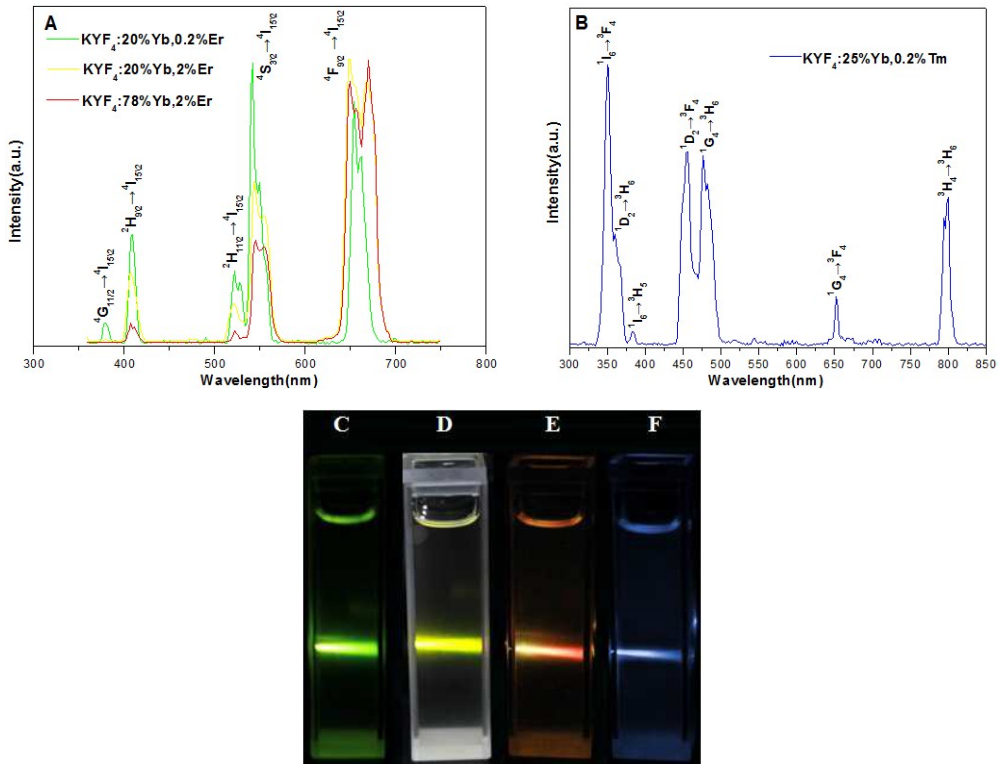

Fig.4 UC luminescence spectra of the Yb,Er/Tm-codoped KYF_4 NCs: (A)KYF_4:20%Yb,0.2%Er, KYF_4:20%Yb,2%Er, KYF_4:78%Yb,2%Er, and KYF_4:25%Yb,0.2%Tm. (B)The photographs show the corresponding 1wt% ethanol solutions of (C)KYF_4:20%Yb,0.2%Er, (D)KYF_4:20%Yb,2%Er, (E)KYF_4:78%Yb,2%Er, and (F)KYF_4:25%Yb,0.2%Tm.The colloidal NCs were excited with 980nm laser under power density of 2 W/cm^2

Fig.4B shows UC luminescence spectra of Yb,Tm-codoped KYF_4 NCs. Under the 980nm near-infrared excitation, the Tm^{3+}/Yb^{3+}-codoped KYF_4 colloidal NCs dispersed in the 1 wt% ethanol display unexpected up-conversion emission spanning the UV-to-NIR regions, which emerge from all the energy transfer of Tm^{3+} ions . Interestingly, two intense emission peaks and one weak peak at 350, 360, and 382nm occurred in the UV emission region, which are generated from the electronic transition of $^1I_6 \rightarrow {}^3F_4$, $^1D_2 \rightarrow {}^3H_6$, and $^1I_6 \rightarrow {}^3H_5$, respectively. In the visible wavelength range, two strong blue peaks located at 456 and 476nm, and a red peak located at 652nm, which were attributed to electronic level transitions of $^1D_2 \rightarrow {}^3F_4$, $^1G_4 \rightarrow {}^3H_6/{}^3F_4$ of the Tm^{3+} ions, respectively. Because of the population of $^1D_2$ level of Tm^{3+} ions is not restrained, the $^1D_2$ level of Tm^{3+} is unable to transfer the fourth photon from the energy level of Yb^{3+} to the energy of $^1G_4$ level. Therefore, the cross relaxation (CR) process of $^3F_2 + {}^3H_4 \rightarrow {}^3H_6 + {}^1D_2$ between Tm^{3+} ions may alternatively play an important role in populating the $^1D_2$ level[36]. In the NIR region, one emission at 800nm is again observed, corresponding to electronic level transitions of $^3H_4 \rightarrow {}^3H_6$ of the Tm ions. As shown in Fig.4F. KYF_4:25%Yb, 0.2%Tm solution emits the strong blue up-conversion luminescence, which can be explained by the energy transfer mechanism of Tm^{3+} ions derived in the Fig.3.

From what has been discussed above，the Yb^{3+} and Er^{3+} doped ion concentration caused little change in the position of the characteristic emission peak, which is determined by Er^{3+} photons number. Therefore, it is necessary to study the relationship between the pumping power density (I_{IR}) and the UC emission intensities

(I_{UC}) to determine the number of photons involved in the UC process. In general, the UC emission intensity (I_{UC}) is expected to be directly proportional to the *n*th power of the excitation power (I_{IR}):I_{UC}~I_{IR}^{n}, where *n* is the absorbed photon numbers (>1) per visible photon emitted, and its value can be obtained from the slope of the fitted line of the plot of log (I_{UC}) versus log (I_{IR}) [32].

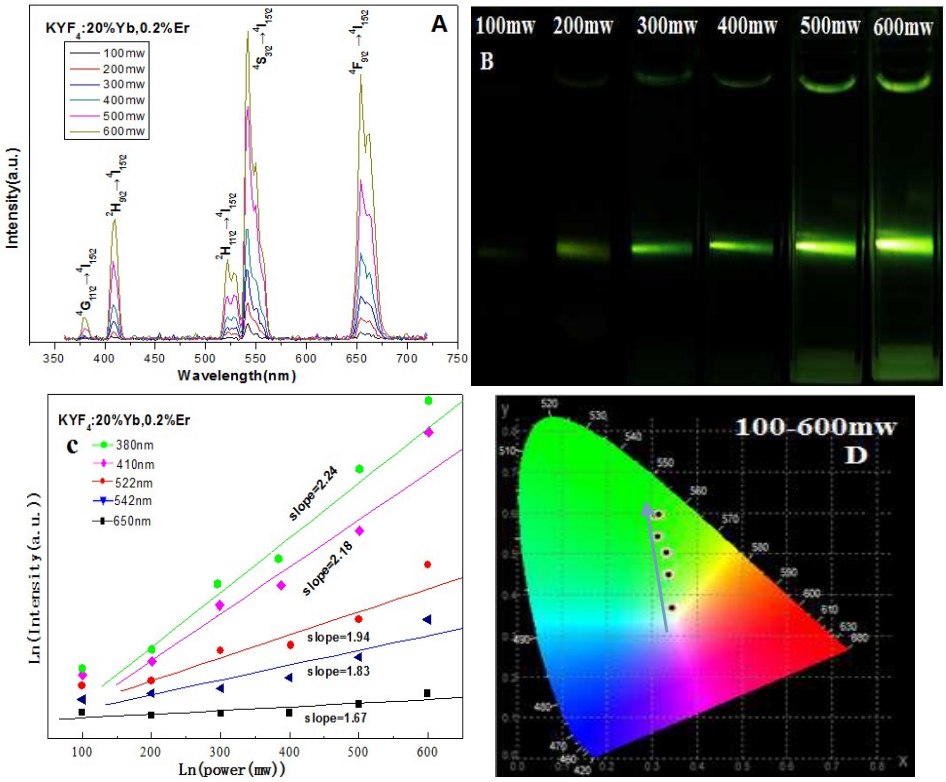

Fig.5. (A) UC luminescence spectra of the KYF_4:20%Yb,0.2%Er NCs excited with 980nm diode laser with power density of 100 to 600mW/cm^2, **(B)** Luminescence photographs of the corresponding KYF_4:20%Yb^{3+},0.2%Er^{3+} samples dispersed in 1wt% ethanol colloidal solutions under 980nm laser excitation with power density of 100 to 600mW/cm^2, **(C)**Log–log power dependence of the UC emissions of KYF_4:20%Yb,0.2%Er NCs, and (D)CIE(X, Y) coordinate diagram showing the chromaticity points calculated from the UC emission spectra of KYF_4:20%Yb,0.2%Er NCs excited under a 980nm laser

Fig.5 A and B show the UC spectra and the corresponding to luminescence photographs of KYF_4:20%Yb,0.2%Er NCs excited with a 980nm diode laser with power density of 100-600 mW/cm^2. Fig. 5C shows the log(I_{UC})–log(I_{IR}) plots of emission intensity and excitation power . The slopes of the linear fits of log (I_{UC})

versus log (I_{IR}) for the UV, blue, green, and red emissions at 380, 410, 522, 542, and 650nm in the KYF_4:20%Yb,0.2%Er sample are 2.24, 2.18, 1.94, 1.83, and 1.67, respectively. These results indicate that emission peaks at 650, 542, and 522nm are attributed to 2-photon up-conversion process, while these peaks at the spectrum of 410 and 380 nm emerge via 3-photon up-conversion process, which are consistent with previous reports on $NaYF_4$[24], $RbGdF_4$[37], $NaGdF_4$[38] NCs. As shown in Fig.3, the potential upconversion energy-mechanisms from the Yb^{3+}/Er^{3+} co-doped KYF_4 NCs are illustrated by simplified energy level diagrams. Fig.5D clearly shows the calculated color coordinates and the CIE 1931 chromaticity diagram of the Yb^{3+}/Er^{3+} codoped KYF_4 NCs for the UC emissions at various powers. When the laser power changed from 100 to 600 mW, the CIE color coordinates of the UC emission of Yb^{3+}/Er^{3+} co-doped KYF_4 NCs shifted from whitish green to the bright green region.

Transition between yellow and red emissions by the host element Yb^{3+} instead of Y^{3+} also observed in the Fig. 4A, indicating that the change of Yb^{3+} concentrations can affect color output. Therefore, it is necessary to further study influence of Yb^{3+} doped concentration on light-emitting properties of β-KYF_4 nanocrystals.

Fig.6A,B show the UC spectra and the luminescence photographs of KYF_4: x% Yb^{3+}, 2% Er^{3+} with different concentrations of Yb^{3+} ion. As can be seen from Fig.6A, the position of band peaks have no obvious change among the four colloidal samples dispersed in ethanol (1 wt%) solution with the increase of Yb^{3+} concentration. The content of Yb^{3+} increase resulted in the decrease of relative peak intensity at 380nm UV ($^4G_{11/2}\rightarrow{}^4I_{15/2}$), 410nm blue ($^2H_{9/2}\rightarrow{}^4I_{15/2}$) and 522, 542 nm green

($^2H_{11/2}$,$^4S_{3/2}$→$^4I_{15/2}$) light emissions. When the doped Yb^{3+} concentration changed from 20% to 50%, they both finally emitted the bright yellow light, as shown in Fig. 6B. Interestingly, the intensity of the 668 nm red emissions was slightly enhanced by increasing the Yb^{3+} concentration. When the doped Yb^{3+} concentration increased to 78%, the red emission become the primary colors, which is quite similar to previous reports of Yb^{3+}/Er^{3+} codoped $NaYF_4$[21] and $NaLuF_4$[26].

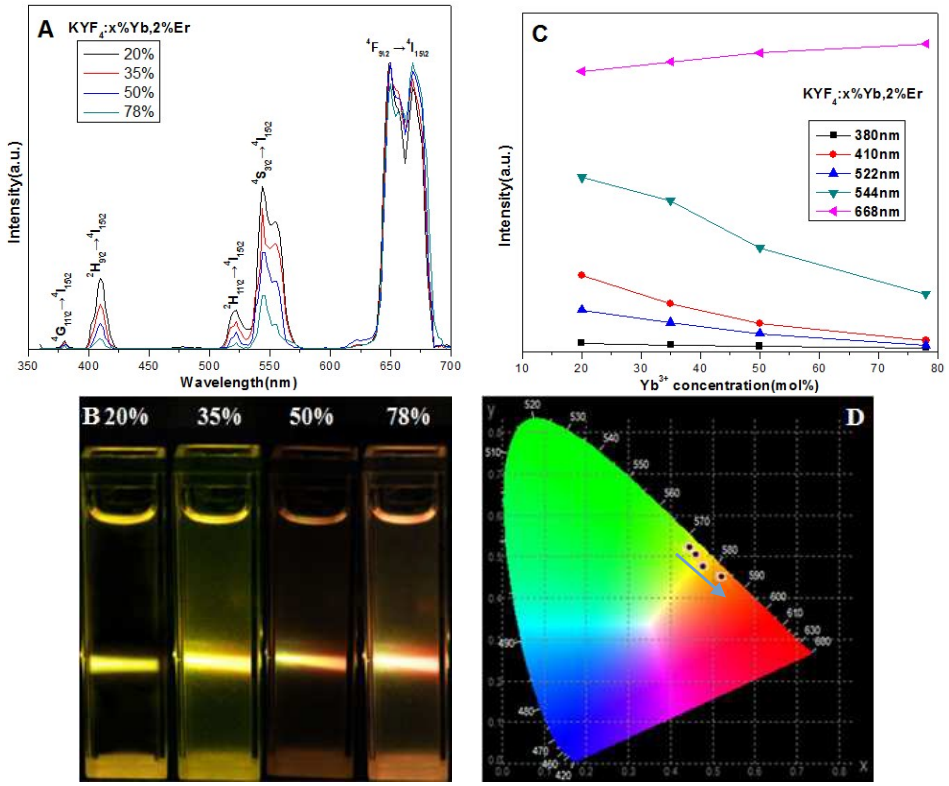

Fig.6. (A) UC luminescence spectra of the KYF_4:x%Yb,0.2%Er NCs (x=20, 35, 50, and 78)excited with 980 nm diode laser. **(B)** luminescence photographs of the corresponding KYF_4:20%Yb^{3+},0.2%Er^{3+} samples dispersed in 1 wt % ethanol colloidal solutions under 980 nm laser excitation with a power density of 2W/cm^2. **(C)** Log−log power dependence of the UC emissions of KYF_4:x%Yb,0.2%Er NCs, and (D) CIE (X,Y) coordinate diagram showing the chromaticity points calculated from the UC emission spectra of KYF_4:x%Yb,0.2%Er NCs excited under a 980nm laser.

In order to deeply investigate the involved UC mechanism in KYF_4:x% Yb^{3+},2% Er^{3+}, the log(I_{UC})–log(I_{IR}) plots of emission intensity and excitation power are shown

in Fig. 6C. The slope of the fitted line of the plot of log (I_{UC}) versus log (I_{IR}) for the UV, blue, and green emission intensity in KYF_4:x% Yb^{3+},2% Er^{3+} samples are negative, while red emission intensity gradually increase with the content of Yb^{3+} increases. As reported UC mechanism in KYF_4:Yb^{3+}/Er^{3+}, only 2-photon emission process involves the production of green and red UC, UC and 3-photon processes is the need for UV and blue emission. Based on above discusses, we explain UC mechanism in KYF_4:Yb^{3+}, Er^{3+} with different Yb^{3+} concentration. With the amount of Yb^{3+} dopants increase in the KYF_4 host lattice, the Yb-Er inter-atomic distance will be decreased to facilitate back-energy-transfer from Er^{3+} to Yb^{3+}, which will subsequently suppress the population in excited levels of $^4G_{11/2}$, $^2H_{9/2}$, $^2H_{11/2}$ and $^4S_{3/2}$ and result in the decrease of UV ($^4G_{11/2}\rightarrow{}^4I_{15/2}$),blue ($^2H_{9/2}\rightarrow{}^4I_{15/2}$), and green ($^2H_{11/2}$, $^4S_{3/2}\rightarrow{}^4I_{15/2}$) emissions. In addition, the energy-transfer from Yb^{3+} to Er^{3+} results in the saturation of the $^4I_{13/2}$ (Er^{3+}) state, and then energy of the excited Yb^{3+} ions transfer to Er^{3+} ions through the anti-stokes emission process $^2F_{5/2}(Yb^{3+})$ + $^4I_{13/2}(Er^{3+})\rightarrow{}^2F_{7/2}(Yb^{3+})$ + $^4F_{9/2}(Er^{3+})$, which can be directly filled in the $^4F_{9/2}$ level, resulting in the enhancement of red emission ($^4F_{9/2}\rightarrow{}^4I_{15/2}$). The chromaticity coordinates shift slowly to red region with the increasing of Yb^{3+} concentration, indicating that luminescent colors can be adjusted in a wider range. Fig.6D shows the calculated color coordinates and CIE 1931 chromaticity diagram of KYF_4:x% Yb^{3+},2% Er^{3+} (x=20, 35, 50, and 78) under 980 nm laser excitation, which vividly describes the change in crystal color trends by adjusting Yb^{3+} concentrations. In short,

the upconversion luminescent output colors of KYF_4:Yb^{3+},Er^{3+} can be changed from yellow to red emission with the increasing of Yb^{3+} concentration.

4. Conclusions

In conclusion, we have successfully synthesized pure hexagonal phase β-KYF_4 NCs with a good monodispersity by a trifluoroacetates thermolysis method using oleic acid and octadecylene as a coordinate solvent. The microstructure and nanoparticle size of KYF_4:Yb,Er/Tm NCs were characterized using XRD and TEM. The average particle size was 18 nm for the β-KYF_4:20% Yb,2% Er NCs and 20 nm for the β-KYF_4:20% Yb,0.2% Tm NCs. The optical properties of the β-KYF_4 doped with various lanthanide ions (Ln^{3+}=Yb^{3+},Er^{3+}, and Tm^{3+}) were investigated under 980 nm excitation. The colloidal KYF_4:Yb, Er/Tm NCs exhibit strong multiple up-conversion emission spanning from the deep UV-to-NIR region (300-850nm) with 980nm laser excitation. It is shown that the as-synthsized β-KYF_4 NCs can emit the bright eye-visible blue, green, yellow, and red emissions by adjusting concentration of Yb^{3+} and activator ions (Er^{3+} or Tm^{3+}). Moreover, the UC luminescent colors can be tuned for the four basic colors from blue to green to yellow and finally to red emission in the β-KYF_4:X%Yb^{3+}/(0.2%-2%)Er^{3+} and β-KYF_4: 25% Yb^{3+}/0.2% Tm^{3+} colloidal samples. This work substantially expands our understanding of this category of KYF_4 upconversion nanocrystals .

Acknowledgements

This work was supported by National College Students' innovation and entrepreneurship training plan of China (20141049701020), self-determined and

innovative research funds from Wuhan University of Technology(grant number 146801006) and Wuhan Municipal Science and Technology Bureau, China (grant No. 2015010101010006).

Notes and references

1 N. Niu, P. Yang, F. He, X. Zhang, S. Gai, C. Li and J. Lin, *J. Mater. Chem.,* **2012**, *22*, 10889-10899.

2 F. Zhang, G. B. Braun, Y. F. Shi, Y. C. Zhang, X. H. Sun, N. O. Reich, D. Zhao and G.Stucky, *J. Am. Chem. Soc.,* 2010, **132**, 2850-2851.

3 F. Zhang, G. B. Braun, A. Pallaoro, Y. Zhang, Y. Shi, D. Cui, M.Moskovits, D. Zhao, G. Stucky, *Nano Lett.,* 2012, **12**, 61-67.

4 F. Zhang, Q. Shi, Y. Zhang, Y. Shi, K. Ding, D.Zhao and Stucky, G. *Adv. Mater.,* 2011, **23**, 3775-3779.

5 S. Han, R. Deng, X. Xie and X. Liu, *Angew. Chemie Int. Ed.* 2014, **53**, 11702-11715.

6 H. Wang, M. Batentschuk, A. Osvet, L. Pinna and C. Brabec, *J. Adv. Mater.,* 2011, **23**, 2675-2680.

7 G. Y. Chen, J. Shen, T. Y. Ohulchanskyy, N. J. Patel, A. Kutikov, Z. Li, J. Song, R. K. Pandey, H. Agren, P. N. Prasad and G. Han, *ACS Nano.,* 2012, **6**, 8280-8287.

8 X. Li, D. Shen, J. Yang, C. Yao, R. Che, F. Zhang and D. Zhao, *Chem. Mater.,* 2013, **25**, 106-112.

9 J. I. Cutler, E. Auyeung, C. A. Mirkin, *J. Am. Chem. Soc.,* 2012, **134**, 1376-1391.

10 J.-H. Lee, G.-H. Kim, J.-M. Nam, *J. Am. Chem. Soc.,* 2012, 134, 5456-5459.

11 Y. Wang, G. Chen, M. Yang, G. Silber, *Nat. Commun.,* 2010, **1**, 87.

12 F. Auzel, *Chem. Rev.,* 2004, **104**, 139-173.

13 H. Zhu, X. Chen, L. M. Jin, Q. J. Wang, F. Wang and S. F. Yu, *ACS Nano.,* 2013, **7**, 11420-11426.

14 J.Pichaandi, J. C. Boyer, K. R. Delaney and F.C.J.M. van Veggel, *J. Phys. Chem. C,* 2011, **115**, 19054-19064.

15 F.Wang and X. G. Liu, *Chem. Soc. Rev.,* 2009, **38**, 976-989.

16 M. Pedroni, F. Piccinelli, T. Passuello, S. Polizzi, J.Ueda, P. Haro-González, L. Martinez Maestro, Jaque D. , J.García-Solé, and A. Speghini, *Cryst.* M. Bettinelli *Growth Des.* 2013, **13**, 4906-4913.

17 F. Wang, Han, Y. C. S. Lim, Y. Lu, J. Wang, J. Xu, H. Chen, C. M. Zhang, *Nature,* 2010, **463**, 1061-1065.

18 W. Zou, C. Visser, J. A. Maduro, M. S. Pshenichnikov and J. C.Hummelen, *Nat. Photon.,* 2012, **6**, 560-564.

19 C. X. Li and J. Lin, *J. Mater. Chem.,* 2010, **20**, 6831-6847.

20 S. J. Budijono, J. Shan, N. Yao, Y. Miura, T.Hoye, R. H. Austin, Y. Ju and R. K. Prud'homme, *Chem. Mater.,* 2009, **22**, 311-318.

21 X. Teng, Y. Zhu, W. Wei, S. Wang, J. Huang, R. Naccache, W.Hu, A. I. Y.Tok, Y. Han, Q.Zhang, Q. Fan, W. Huang, J. A. Capobianco and L. Huang, J. Am. Chem. Soc., 2012, 134, 8340-8343.

22 Q. Su, S. Han, X. Xie, H. Zhu, H. Chen, C. Chen, R. Liu, X. Chen, F.Wang and X. Liu, *J. Am. Chem. Soc.,* 2012, **134**, 20849-20857.

23 C. T. Xu, P. Svenmarker, H. C. Liu, X. Wu, M. E. Messing, L. R.Wallenberg and S.A. Engels, ACS Nano., 2012, 6, 4788-4795.

24 K. W. Krämer, D. Biner, G. Frei, H. U. Güdel, M. P.Hehlen and S. R. Lüthi, *Chem. Mater.* 2004, **16**, 1244-1251.

25 G.Z. Ren, S. J. Zeng and J. H. Hao, *J. Phys. Chem. C* 2011, **115**, 20141 – 20147.

26 H. Schäfer, P. Ptacek, O. Zerzouf and M.Haase, *Adv. Funct. Mater.,* 2008, **18**, 2913-2918.

27 J. Méndez-Ramos, A. C. Yanes, A. Santana-Alonso and J. del-Castillo, *Chemical Physics Letters,* 2013, **555**, 196-201.

28 A. C. Yanes, A. Santana-Alonso, J. Mendez-Ramos and J. del-Castillo, *Appl. Phys. B.* **2013**, *113*, 589-596.

29 V. N. Makhov, A. S. Vanetsev, N. M. Khaidukov, M.Yin, X. T. Wei, A. Kotlov and A. N. Belsky, *Radiation Measurements,* 2013, **56**, 393-396.

30 E. M. Chan, G. Han, J. D. Goldberg, D. J. Gargas, A. D. Ostrowski, P. J. Schuck, B. E. Cohen and D. J.Milliron, *Nano Lett.,* **2012**, *12*, 3839-3845.

31 X. Li, F. Zhang and D. Zhao, *Nano Today,* 2013, **8**, 643-676.

32 F.Wang and Liu, X. *J. Am. Chem. Soc.,* 2008, **130**, 5642-5643.

33 H. Schäfer , C. Hess , H. Tobergte , A. Volf , S. Ichilmann , H. Eickmeier , B. Voss , N. Kashaev , J. Nordmann , W. Akram , H.-A. Brigitte and M. Steinhart, *small,* 2015, **11**, 931-935.

34 G. S. Yi and G. M. Chow, *Adv. Funct. Mater.,* 2006, **16**, 2324 – 2329.

35 V. Mahalingam, F. Vetrone, R. Naccache, A. Speghini and J. A. Capobianco, *Adv.Mater.*, 2009, **21**, 4025-4028.

36 S. Zeng, G. Ren, W. Li, Ch. Xu and Q. Yang, *J. Phys.Chem. C,* 2010, **114**, 10750-10754.

37 S. Ahmad, R.Nagarajan, P.Raj and G.V. Prakash, *Inorg. Chem.* 2014, ***53***, 10257-10265.

38 G. Ren, S. Zeng, J. Hao, *J. Phys. Chem. C,* 2011, **115**, 20141-20147.